Springer

KSME

Journal of Mechanical Science and Technology 28 (11) (2014) 4613~4620
www.springerlink.com/content/1738-494x
DOI 10.1007/s12206-014-1029-y

Numerical and experimental method to determine the boring diameters of a two-stage TBM cutterhead to prevent rock burst †

Geng Qi*, Wei Zhengying and Meng Hao

State Key Laboratory of Manufacturing System Engineering, Xi'an Jiaotong University, Xi'an, China

(Manuscript Received April 7, 2014; Revised June 28, 2014; Accepted July 30, 2014)

Abstract

A two-stage tunnel boring machine (TBM) cutterhead with a pilot-enlargement boring method was presented to reduce the risk of rock bursts resulting from boring with a TBM with a large flat-face cutterhead. A reduced scale similarity experiment was designed on rock tunnel boring to determine the boring diameters of the two stages, and numerical simulation models were built. A micron X-ray computerized tomography system was adopted to examine the failure area of the excavated testing piece and validate the numerical models. Stress distribution and energy release rate (ERR) were used in the numerical simulations to evaluate the rock burst risk of the boring process. Experimental and numerical results show that rock burst is prone to occur in the upper, lower, and side areas of the surrounding rock around the tunnel, and risk increases with the lateral pressure coefficient and boring diameter. The optimal boring diameter ratio of stages 1 to 2 was determined between 0.55 and 0.59. Meanwhile, the ERR of the designed two-stage cutterhead is approximately 60% smaller than that of the flat-face cutterhead.

Keywords: Rock burst risk; Two-stage TBM cutterhead; Similarity experiment; Energy release rate; Boring diameter ratio

1. Introduction

Tunnel boring machines (TBMs) are heavy-duty engineering machines for boring tunnels. TBMs exhibit high advance rates, excellent working safety, and slight disturbance on excavation zones; they have been widely applied in subway, railway, and water-electricity tunnel projects [1-3]. However, rock bursts are commonly observed in TBM tunnels because the process slightly disturbs surrounding rocks, which leads to low initial release of strain energy [4]. Residual energy contributes to rock bursts. Rock bursts frequently cause serious casualties and equipment failures, which result in increased construction costs or even abandonment of tunnel projects.

Rock burst prevention methods are classified into three types: (1) optimization of excavation and pillar layout schemes, (2) surrounding rock mass support, and (3) pretreatment method [5-7]. Destress blasting, fluid injection into faults, and pilot tunnel boring methods are typically adopted for tunnels with large cross sections [5, 7-10]. These pretreatment techniques depend on excavation methods such as drilling and blasting (D&B) or TBM. A tunnel face with a cross section of over 200 m^2 was bored using TBM pilot and D&B enlargement methods for the new Tomei-Meishin Expressway Tunnel from Tokyo to Kobe [11, 12]. D&B pilot and TBM enlargement methods were successfully applied to the deep tunnel sections of the headrace tunnel of the Jinping II Hydropower Station (Sichuan, China), which is prone to extremely intense rock bursts [7, 8]. Several rock burst risk evaluation indices have been presented, including the failure approaching index [13, 14], energy release rate (ERR) [15], and excess shear stress [16]. ERR has become the most widely used index for evaluating the risk of strain bursts to intact rock masses [5].

Based on our previous research [17-20], we combined the advantages of the fast advancing rate of a TBM and the capability of a TBM pilot to release strain energy in advance; the two-stage TBM cutterhead was invented based on the flat-face cutterhead and the pilot-enlargement boring method [17]. An experimental and numerical method for determining the boring diameters of the two-stage TBM cutterhead was proposed. Numerical models were built to calculate ERR when a TBM bores with stage-1 and stage-2 cutterheads. A reduced scale similarity experiment was designed on tunnel boring to study the rock burst process. The experiment also validated the feasibility of the numerical models. The numerical results show that the optimal boring diameter ratio of stages 1 to 2 varied between 0.55 and 0.59. Meanwhile, the ERR of the two-stage cutterhead is approximately 60% smaller than that of a flat-face cutterhead.

*Corresponding author. Tel.: +86 82665064, Fax.: +86 82660114
E-mail address: gengqi8902@gmail.com
† Recommended by Associate Editor Seong Beom Lee

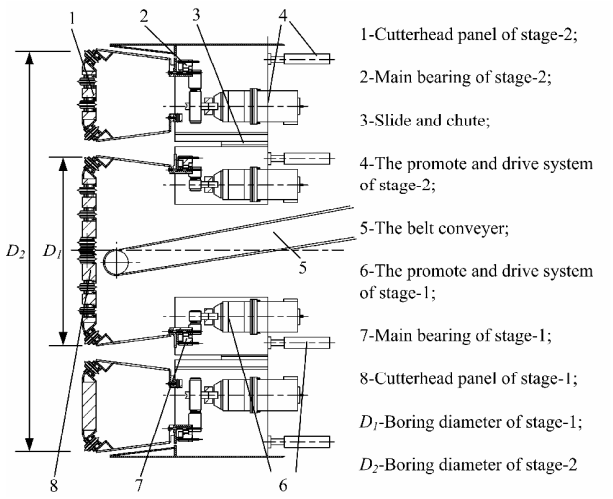

Fig. 1. Basic structure of the two-stage cutterhead.

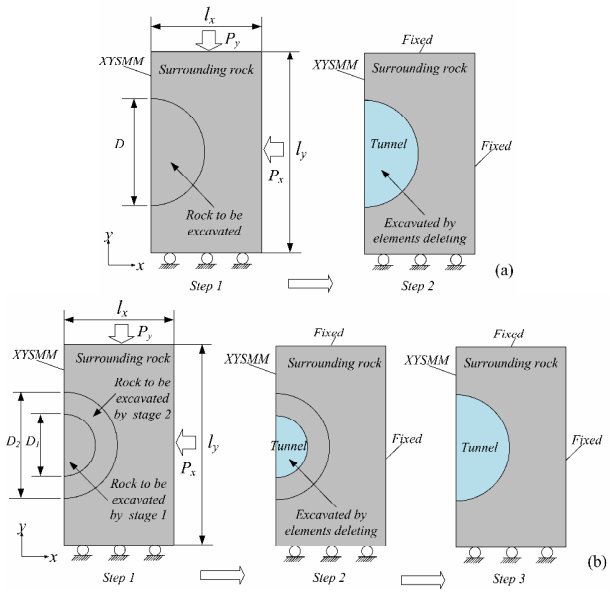

Fig. 2. Geometries and boundary conditions used in the numerical models: (a) bored by the flat-face cutterhead; (b) bored by the two-stage cutterhead, where l_x and l_y are the rock model dimensions; and D, D_1, and D_2 are the boring diameters (m).

2. Numerical models

2.1 Basic structure of the two-stage cutterhead

As shown in Fig. 1, the two-stage cutterhead comprises a flat-face cutterhead (stage 1) installed concentrically with a cylinder (stage 2). Both stages are equipped with their respective driving and promoting systems. The stage-1 cutterhead system can slide inside the stage-2 cutterhead system through the relative motion of the slides installed on the shield of the stage-1 system and the chutes installed on the inner shield of the stage-2 system. The belt conveyer is installed within the stage-1 cutterhead. Rock mucks can be conveyed through the muck holes on the cutterhead support ring.

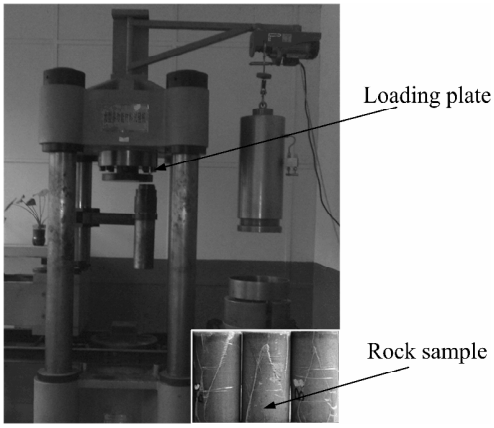

Fig. 3. Multifunctional material testing machine at the geotechnical and rock mechanics laboratory of Xi'an Jiaotong University of Technology, Xi'an, China.

2.2 Setup of the numerical models for the boring process

The 2D axisymmetric models (y axis) of rock tunnel boring were built within the virtual space of ABAQUS. The geometries and boundary conditions of different analysis steps are shown in Fig. 2. The boring process of the flat-face cutterhead consists of two steps. In step 1, the axially symmetric boundary condition (*XSYMM*) was applied to the left edge of the model. Pressures P_x (Mpa) and P_y (Mpa), which represent horizontal and vertical ground stresses, were applied on the top and right edges of the model, respectively. In step 2, the pressures were removed and the fixed boundary condition was applied to the top and right edges. Meanwhile, the semicircular area was deleted using an ABAQUS element removal technique to simulate the rock excavation process. Prior to removal, the forces exerted on the remaining part of the model were stored in the nodes of the boundary between them. These forces were ramped down to zero during removal, and the remaining model was calculated to reach a new balance according to the mechanical balance, deformation coordination, and material constitutive laws [21-23]. The boring process of the two-stage cutterhead consists of three steps. In these steps, the applied pressures and boundary conditions were similar to those of the model of the flat-face cutterhead. The rock excavation process consists of two steps, which represent the boring of stage-1 and stage-2 cutterheads.

The numerical models used hard sandrock, which is the same as that in the experiment in Chapter 3. The main rock mechanical properties were tested on a multifunctional material testing machine (Fig. 3) and listed in Table 1. The Drucker-Prager yield function was adopted to describe the elasto-plastic behavior of the rock model.

2.3 Data acquisition during simulations

ERR was used to evaluate the rock burst risk of the surrounding rock, and is calculated as follows:

Table 1. Main mechanical properties of the rock samples.

Density, ρ (kg/m^3)	2500
Uniaxial compressive strength, S_C (Mpa)	78
Brazilian tensile strength, S_T (Mpa)	6
Internal friction angle, φ (°)	38
Young's modulus, E (GPa)	50
Poisson's ratio, ν	0.25

$$ERR = \frac{8\Delta E_S}{8l_x l_y - \pi D^2}, \tag{1a}$$

$$ERR_1 = \frac{8\Delta E_{S1}}{8l_x l_y - \pi D_1^2}, \tag{1b}$$

$$ERR_2 = \frac{8\Delta E_{S2}}{8l_x l_y - \pi D_2^2}, \tag{1c}$$

where ΔE_S, ΔE_{S1}, and ΔE_{S2} are the released strain energies from the surrounding rock; l_x and l_y are the width and height of the model, respectively; and D, D_1, and D_2 are the boring diameters of the flat-face, stage-1, and stage-2 cutterheads, respectively.

The ERRs of the boring processes by the flat-face, stage-1, and stage-2 cutterheads were calculated using Eqs. (1a), (1b), and (1c), respectively.

The value of ΔE_S must first be obtained from the numerical simulations to calculate ERR.

The history output option of the total strain energy was adopted in the analysis to obtain the value of ΔE_S.

3. Experiments

3.1 Equipment of reduced scale similarity tunnel boring test

Similarity tunnel boring test was conducted on the planar biaxial testing machine (Fig. 4) in the mechanical testing and simulation (MTS) demonstrative center of Xi'an Jiaotong University, Xi'an, China. The loading capacity of the equipment is 100 KN. The data acquired from the test included forces and deformation. The biaxial testing machine exerted a load on the four side faces of the testing sample, and the pressure shaft was controlled with loading and displacement methods.

3.2 Sample preparation

As shown in Fig. 5, the testing sample was designed to consist of the surrounding rock and rock core assembled via cylinder assembly. The surrounding rock is the residual part of a complete cuboid rock piece after it was trepanned. The dimensions of the cuboid rock piece are 100 mm × 100 mm × 25 mm, and the diameters of the cylinder hole and core are 82 mm and 74 mm, respectively. The cylinder assembly consisted of internal and external cones that were introduced to achieve the rock excavation process under ground stress. The structure of the cylinder assembly is shown in Fig. 6. The

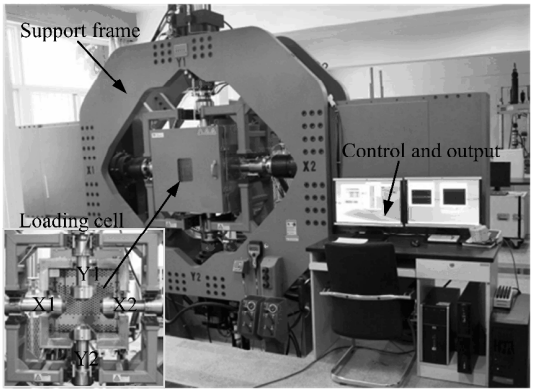

Fig. 4. Planar biaxial testing machine in the MTS demonstrative center of Xi'an Jiaotong University.

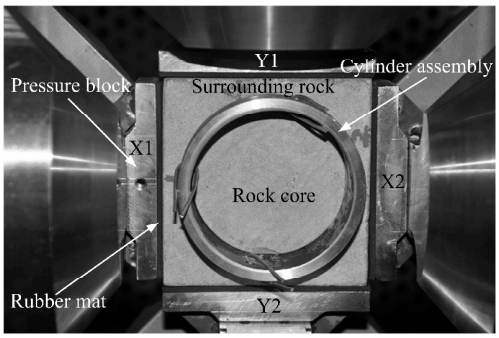

Fig. 5. Testing sample and the assembled and clamped method.

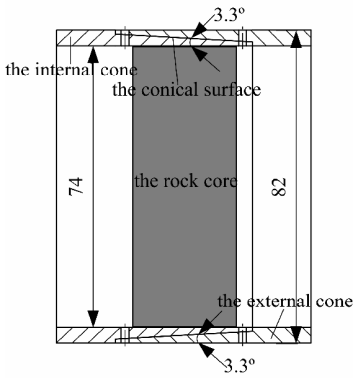

Fig. 6. Cylinder assembly and rock core.

internal surface of the internal cone is a cylindroid with a diameter of 74 mm, and the external surface is conical with a conical degree of 3.3°. The external surface of the external cone is a cylindroid with a diameter of 82 mm, and the internal surface is conical with a conical degree of 3.3°. The two conic surfaces can fit completely and separate easily. The testing sample was clamped by the pressure blocks (X1, X2, Y1, and Y2). A piece of 2 mm-thick rubber mat was attached to the pressure surface of each pressure block to ensure uniform pressure on the testing sample.

Two numerical models of sample tunnel boring were built to determine the material of the cylinder assembly. The cylinder material was set as steel or aluminum (Al) alloy. No plas-

Table 2. Mechanical properties of rock and cone materials.

Properties	Sandstone	Al alloy	Steel
Density, ρ (kg/m^3)	2500	2700	7800
Young's modulus, E (GPa)	50	70	210
Poisson's ratio, ν	0.25	0.33	0.3
ERR (J/m^3)	259.8	270.7	304.4

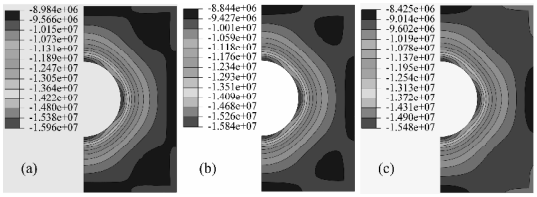

Fig. 7. Contours of the maximum principal stress with different cylinder materials: (a) no cylinder; (b) Al-alloy cylinder; (c) steel cylinder (compression, Pa).

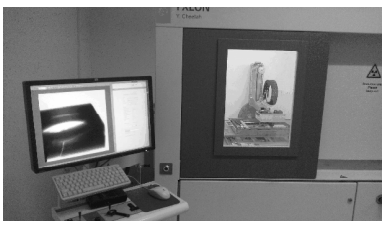

Fig. 8. Examination of the surrounding rock on the micron X-ray computerized tomography system.

tic deformation occurred in the cylinder assembly before rock failure, and thus, only the elastic properties were considered. The mechanical properties and ERR results are listed in Table 2, and the contours of the maximum principal stress are shown in Fig. 7. ERR error between the Al-alloy cylinder model and the no-cylinder model is 4.2%, which is smaller than the 17.2% error of the steel cylinder model. Moreover, the stress contour of the Al-alloy cylinder model is closer to the no-cylinder model than the steel cylinder model. Consequently, the cone material was chosen as the Al-alloy.

3.3 Testing procedure and observation

The testing procedure included two steps: loading and excavation. During loading, the displacement of the Y2 pressure block was maintained at zero and the other pressure blocks were loaded with a loading rate of 500 N/s. After the load was applied to a given value and kept constant for 2 min, the displacements of the four pressure blocks were maintained at zero. During excavation, the cylinder assembly and rock core were removed by separating the fitted conical surfaces. The displacements of the four pressure blocks were maintained at zero for another 5 min after excavation. The surrounding rock was then examined on the micron X-ray computerized tomography system (Fig. 8) to identify which zone of the surrounding rock is prone to failure.

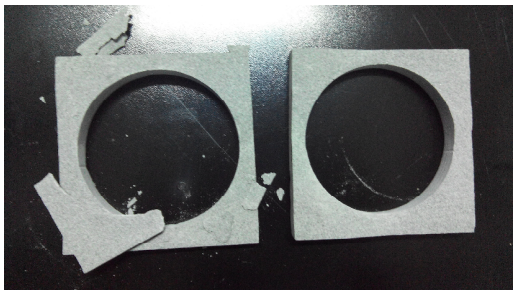

Fig. 9. Photo of the failure in the surrounding rock.

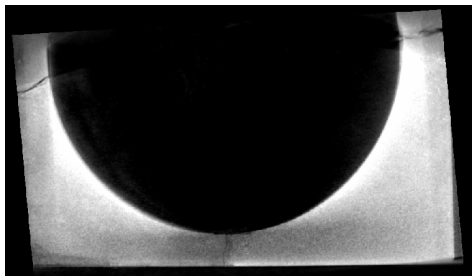

Fig. 10. Micron X-ray photo of the surrounding rock after the test.

4. Results and discussion

4.1 Testing results

According to the similarity criterion for the model test of hydraulic structures, the deformation rule of a testing model should be similar to that of a real model. The deformation similar constant should be equal to the geometry similar constant, which requires the elasticity modulus (E) and strain (ε) of the testing model to be equal to those of the real model. Thus, the pressures applied on the testing model should be equal to those on the real model. In the test, ground stresses P_x and P_y were set to 10 Mpa. The loads of the pressure blocks (X1, X2, and Y1) were 25 KN.

During the load maintenance process, the surrounding rock bursts into two pieces from the center part in the axial direction (Fig. 9). This phenomenon illustrates that the failure of the surrounding rock in the tunnel axial direction is in tensile mode. After the cylinder assembly and cylinder rock core were removed, microcracks initialized in the upper, lower, and side areas of the surrounding rock (Fig. 10). These cracks were caused by the accumulated strain energy released toward the tunnel center.

4.2 Effect of the lateral pressure coefficient on stress distribution

The lateral pressure coefficient (K), which is defined as the ratio of the horizontal ground stress to the vertical ground stress, is formulated as follows:

$$K = \frac{P_x}{P_y}. \tag{2}$$

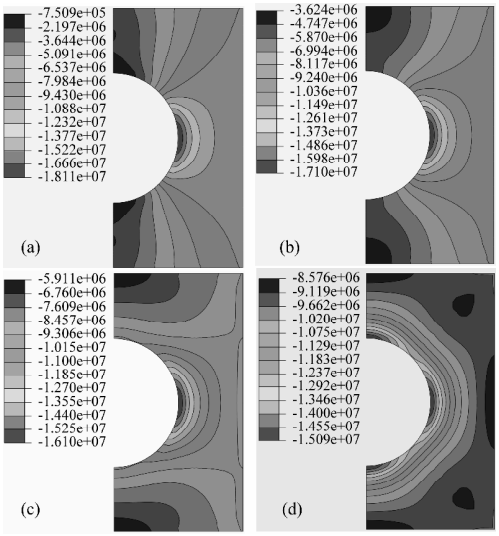

Fig. 11. Contours of the maximum principal stress with different K values (compression, Pa): (a) K = 0.25; (b) K = 0.5; (c) K = 0.75; (d) K = 1.

Simulations were conducted by adopting the numerical models in Fig. 2(a) and assuming that D is equal to 10 m, and P_y is equals to 10 Mpa.

As shown in the stress contours in Fig. 11, the stress around the tunnel wall increases with K; rock burst is prone to occur when K is high. As shown in Fig. 11(d), the highest compression stress appears in the upper, lower, and side areas of the surrounding rock when K is equal to 1, and rock burst is prone to occur in these areas. The simulation is consistent with the experimental results in Fig. 9 and validates the feasibility of the numerical models.

4.3 Effect of the boring diameter of the flat-face cutterhead on ERR

Simulations were conducted when K varied between 0.25 and 1.0 by adopting the numerical models in Fig. 2(a) and assuming that D is equal to 2 m to 10 m, and P_y is equal to 10 Mpa.

As shown in Fig. 12, compressive stress increases with the boring diameter for the corresponding points of the surrounding rock with different boring diameters; a large boring diameter results in great disturbance. As shown in Fig. 13, ERR increases with boring diameter and K value. Rock burst risk increases with boring diameter and K value, which is in accordance with the contour analysis results in Secs. 4.2 and 4.3. Consequently, the two-stage TBM cutterhead with the pilot-enlargement boring method was introduced to reduce the rock burst risk of the large flat-face TBM cutterhead.

4.4 Effect of boring diameters of the two-stage cutterhead on ERR

Pilot-boring by the stage-1 cutterhead releases ground stress in advance. Rock burst risk can be reduced effectively when

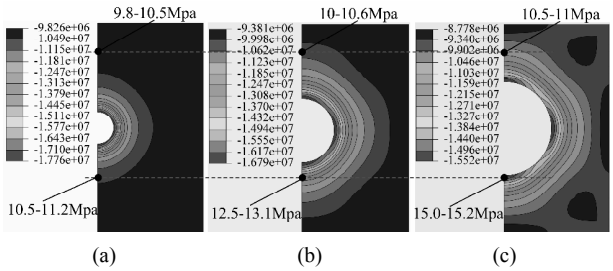

Fig. 12. Contours of the maximum principal stress with different boring diameters and K = 1: (a) D = 3 m; (b) D = 6 m; (c) D = 9 m (compression, Pa).

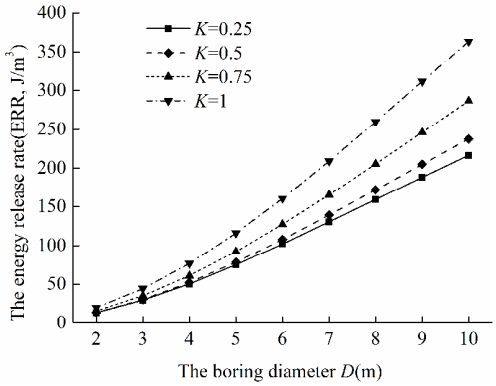

Fig. 13. Effect of the boring diameter of the flat-face cutterhead on ERR with different K values.

the stage-2 cutterhead conducts enlargement-boring. According to the results in Sec. 4.3, rock burst risk from the pilot-boring of the stage-1 cutterhead increases with boring diameter D_1. Consequently, simulations were conducted, which adopted the numerical model in Fig. 2(b), with D_1 varying from 2 m to 8 m and D_2 varying from 7 m to 10 m. Hence, the best boring diameter ratio (D_1/D_2) of the two-stage cutterhead was determined.

As shown in Fig. 14, ERR_1 increases for different D_2 values, whereas ERR_2 decreases with D_1. D_1 was defined as the optimal boring diameter of the stage-1 cutterhead when $ERR_1 = ERR_2$. Rock burst risk for the two stages reached the best balance with this diameter, and the sum of ERR_1 and ERR_2 simultaneously reached a low value. As shown in the simulation results in Fig. 14 and Tables 3-6, the optimal ratio of D_1/D_2 was determined between 0.55 and 0.59. This ratio was unaffected by the lateral pressure coefficient. The ERR of the two-stage cutterhead is approximately 60% smaller than that of the flat-face cutterhead, which illustrates that rock burst risk for the two-stage cutterhead is smaller than that for the flat-face cutterhead.

5. Conclusion

A two-stage TBM cutterhead with pilot-enlargement boring method was presented to prevent rock burst during TBM boring in high ground stress conditions. Numerical simulations on similarity experiment was designed to study the rock burst

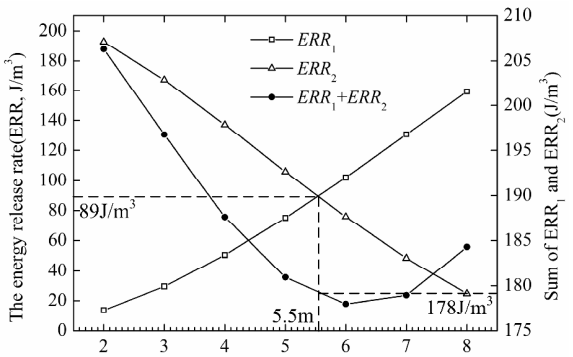

(a) The boring diameter of the stage 1 cutterhead (D_1, m)

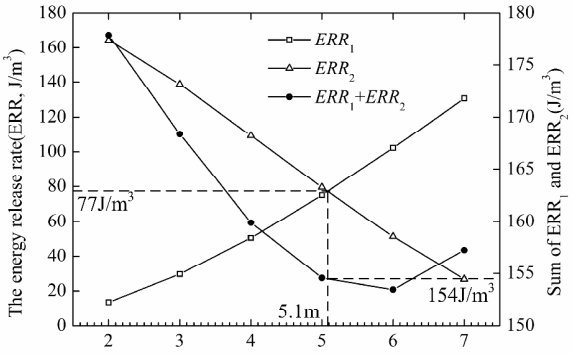

(b) The boring diameter of the stage 1 cutterhead (D_1, m)

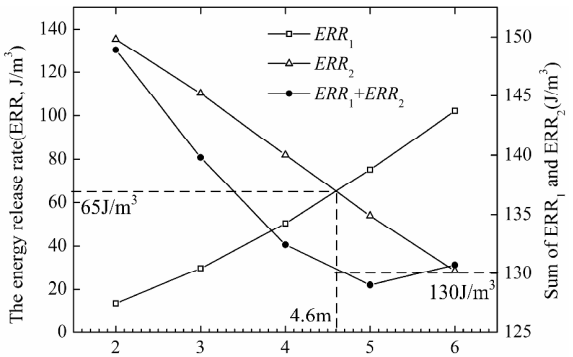

(c) The boring diameter of the stage 1 cutterhead (D_1, m)

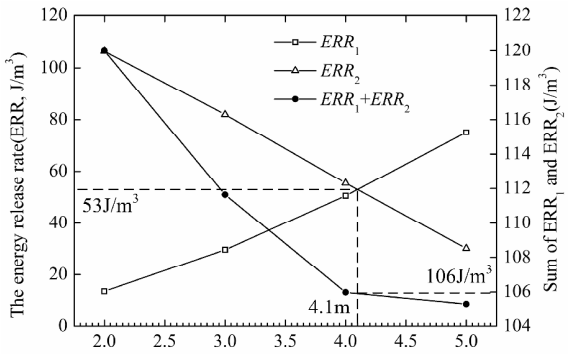

(d) The boring diameter of the stage 1 cutterhead (D_1, m)

Fig. 14. Effects of the boring diameters of the two-stage cutterhead on ERR with $K = 0.25$; the D_2 values are equal to 10, 9, 8, and 7 m for (a), (b), (c), (d), respectively.

Table 3. Simulation results (ERR and optimal D_1/D_2) when $K = 0.25$.

Boring diameter D_2 (m)	10	9	8	7
Optimal boring diameter D_1 (m)	5.5	5.1	4.6	4.1
Optimal ERR_1, ERR_2 (J/m^3)	89	77	65	53
ERR of direct boring with D_2 (J/m^3)	216.4	188.3	159.4	130.5
D_1/D_2	0.55	0.57	0.58	0.59
ERR decrease (%)	58.9	59.1	59.2	59.4

Table 4. Simulation results (ERR and optimal D_1/D_2) when $K = 0.5$.

Boring diameter D_2 (m)	10	9	8	7
Optimal boring diameter D_1 (m)	5.5	5.1	4.6	4.1
Optimal ERR_1, ERR_2 (J/m^3)	95.2	82	69.1	54.8
ERR of direct boring with D_2 (J/m^3)	237.6	204.9	171.9	139.2
D_1/D_2	0.55	0.57	0.58	0.59
ERR decrease (%)	59.9	60.0	59.8	60.6

Table 5. Simulation results (ERR and optimal D_1/D_2) when $K = 0.75$.

Boring diameter D_2 (m)	10	9	8	7
Optimal boring diameter D_1 (m)	5.5	5.1	4.6	4.1
Optimal ERR_1, ERR_2 (J/m^3)	108.5	95.8	81.1	64.4
ERR of direct boring with D_2 (J/m^3)	286.7	246.1	205.3	165.5
D_1/D_2	0.55	0.57	0.58	0.59
ERR decrease (%)	62.2	61.1	60.5	61.1

Table 6. Simulation results (ERR and optimal D_1/D_2) when $K = 1$.

Boring diameter D_2 (m)	10	9	8	7
Optimal boring diameter D_1 (m)	5.5	5.1	4.6	4.1
Optimal ERR_1, ERR_2 (J/m^3)	140.3	121	99.1	80.2
ERR of direct boring with D_2 (J/m^3)	363.6	311.7	259.8	209.0
D_1/D_2	0.55	0.57	0.58	0.59
ERR decrease (%)	61.4	61.2	61.9	61.6

the tunnel boring process were conducted. A reduced scale process during tunnel boring and validate the feasibility of the numerical models.

Failure is prone to occur in the upper, lower, and side areas of the surrounding rock around the tunnel wall when the accumulated strain energy is released toward the tunnel center after excavation.

Rock burst risk was evaluated by the stress distribution and ERR of the surrounding rock. Rock burst risk is closely related to the ground stress condition and increases with the lateral pressure coefficient, which is defined as the ratio of horizontal ground stress to vertical ground stress.

Rock burst risk during TBM boring increases with boring diameter.

The two-stage cutterhead effectively reduced rock burst risk during TBM boring. The optimal boring diameter ratio of

stage 1 to stage 2 was determined between 0.55 and 0.59. This ratio was unaffected by the lateral pressure coefficient. The ERR of the two-stage cutterhead is approximately 60% smaller than that of the flat-face cutterhead.

Acknowledgment

This work was supported by the Major State Basic Research Development Program of China (the 973 Program) (Grant No. 2013CB035402).

References

[1] O. Acaroglu, L. Ozdemir and B. Asbury, A fuzzy logic model to predict specific energy requirement for TBM performance prediction, *Tunnelling and Underground Space Technology*, 23 (2008) 600-608.

[2] J. Huo, W. Sun, J. Chen and X. Zhang, Disc cutters plane layout design of the full-face rock tunnel boring machine (TBM) based on different layout patterns, *Computers & Industrial Engineering*, 61 (2011) 1209-1225.

[3] W. Sun, J. Huo, J. Chen, Z. Li, X. Zhang, L. Guo, H. Zhao and Y. Zhao, Disc cutters' layout design of the full-face rock tunnel boring machine (TBM) using a cooperative coevolutionary algorithm, *Journal of Mechanical Science and Technology*, 25 (2011) 415-427.

[4] Q. Gong, L. Yin, S. Wu, J. Zhao and Y. Ting, Rock burst and slabbing failure and its influence on TBM excavation at headrace tunnels in Jinping II hydropower station, *Engineering Geology*, 124 (2012) 98-108.

[5] M. Board, Numerical examination of mining-induced seismicity, *in: ISRM International Symposium-EUROCK 96*, International Society for Rock Mechanics (1996).

[6] M. Salamon, Energy considerations in rock mechanics: fundamental results, *Journal of the South African Institute of Mining and Metallurgy*, 84 (1984) 233-246.

[7] C. Zhang, X. Feng, H. Zhou, S. Qiu and W. Wu, A top pilot tunnel preconditioning method for the prevention of extremely intense rockbursts in deep tunnels excavated by TBMs, *Rock Mechanics and Rock Engineering*, 45 (2012) 289-309.

[8] D. M. Fang, N. Liu, C. Zhang, W. J. Zhu and X. J. Chen, Rockburst risk control for large diameter TBM boring in high geostress region, *Chinese Journal of Rock Mechanics and Engineering*, 32 (2013) 2100-2107.

[9] A. Roux, E. Leeman and H. Denkhaus, Destressing: a means of ameliorating rockburst conditions. Part I: the concept of destressing and the results obtained from its applications, *JS Afr Inst Min Metall*, 57 (1957) 101-119.

[10] B. Tang, *Rockburst control using destress blasting*, McGill University (2000).

[11] K. Miura, Design and construction of mountain tunnels in Japan, *Tunnelling and Underground Space Technology*, 18 (2003) 115-126.

[12] K. Miura, H. Yagi, H. Shiroma and K. Takekuni, Study on design and construction method for the New Tomei-Meishin expressway tunnels, *Tunnelling and Underground Space Technology*, 18 (2003) 271-281.

[13] C. Zhang, H. Zhou and X. Feng, An index for estimating the stability of brittle surrounding rock mass: FAI and its engineering application, *Rock Mechanics and Rock Engineering*, 44 (2011) 401-414.

[14] C. Zhang, H. Zhou, X. Feng, L. Xing and S. Qiu, Layered fractures induced by principal stress axes rotation in hard rock during tunnelling, *Materials Research Innovations*, 15 (2011) s527-s530.

[15] F. Hill, N. Cook, E. Hoek, P. Jp, W. Ortlepp and M. Salamon, *Rock mechanics applied to study of rockbursts*, South African inst min metall PO BOX 61127 11-13 maclaren st 13th floor-cape towers, Marshalltown transvaal 2107, South Africa (1966).

[16] J. Ryder, Excess shear stress in the assessment of geologically hazardous situations, *Journal of the South African Institute of Mining and Metallurgy*, 88 (1988) 27-39.

[17] Z. Wei, B. Lu, Q. Geng and J. Du, A two-stage cutter head system for the rock tunnel boring machine (TBM), Chinese invention patent, *CN103016016A* (2013).

[18] Z. Wei, B. Lu, Q. Geng and Y. Wang, A multi-stage enlargement cutter head for the shield tunnel machine, Chinese invention patent, *CN102536255A* (2012).

[19] Z. Wei, B. Lu, C. Tan and Y. Wang, A multi-stage separated cutter head for the shield tunnel machine, Chinese invention patent, *CN102536254A* (2012).

[20] Z. Wei, B. Lu, Q. Geng and J. Du, A triple-stage flat face TBM cutter head for the rock tunnel boring machine (TBM), Chinese invention patent, *CN103485778A* (2014).

[21] Z. Wei, B. Lu, C. Tan and J. Du, Faming Zhuanli Shenqing Shuomingshu, *CN103485778A* (2014) (in Chinese).

[22] Element and contact pair removal and reactivation, *Section 11.2.1 of the Abaqus Analysis User's Manual*.

[23] M. Cai, Influence of stress path on tunnel excavation response-numerical tool selection and modeling strategy, *Tunnelling and Underground Space Technology*, 23 (2008) 618-628.

[24] W. Jiang, K. Yahiaoui and F. R. Hall, Finite element predictions of temperature distributions in a multipass welded piping branch junction, *Journal of pressure vessel technology*, 127 (2005) 7-12.

Geng Qi received his B.E. degree from Shandong University, China in 2011. He is currently a Ph.D. candidate in the School of Mechanical Engineering at Xi'an Jiaotong University, China. His research interests include layout optimization and tunnel boring machine (TBM) cutterhead design.

Wei Zhengying received her Ph.D. from the School of Mechanical Engineering, Xi'an Jiaotong University, China in 2003. Dr. Wei is currently a professor and doctoral supervisor in the School of Mechanical Engineering at Xi'an Jiaotong University. Her research interests include the design and manufacture of microfluidic devices and TBM cutterheads.

Meng Hao received his B.E. degree from Shandong University, China in 2013. He is currently a master candidate in the School of Mechanical Engineering at Xi'an Jiaotong University, China. His research interest includes TBM cutterhead design.